Investigation on interfacial defect criticality of FRP-bonded concrete beams

Ao Zhou [a], Renyuan Qin [a], Luciano Feo [b], Rosa Penna [b], Denvid Lau [a, c, *]

[a] Department of Architecture and Civil Engineering, City University of Hong Kong, Hong Kong, China
[b] Department of Civil Engineering, University of Salerno, Via Giovanni Paolo II, 132 - 84084 Fisciano, SA, Italy
[c] Department of Civil and Environmental Engineering, Massachusetts Institute of Technology, Cambridge, MA 02139, USA

ABSTRACT

Bonding fiber reinforced polymer (FRP) has been proven to be an effective and efficient method to strengthen and/or retrofit deficient concrete components and structures. Interfacial defects may easily arise due to improper construction or environmental deterioration during the designed service life and they may cause an unfavorable effect on the local bond behavior and global performance of FRP-bonded concrete systems. However, the information on the interfacial defect effect and the guideline for distinguishing the criticality of interfacial defect is limited, making it difficult to assess the long term integrity. In this study, FRP-bonded concrete beams containing various interfacial defects are under four-point bending test to evaluate the defect effect and determine the interfacial defect criticality from location and size aspects. Meanwhile, finite element models representing different sizes of FRP-bonded concrete beams are built and simulated to study the size effect of beam. Both the experimental observation and numerical results indicate that the deep beam is more sensitive to interfacial defect than normal beam. The threshold for critical interfacial defect varies significantly depending on the beam type and defect location. The small, medium and large categories of interfacial defect can be classified according to the beam type, defect location and defect size sequentially. Different maintenance strategies should be adopted corresponding to small, medium and large interfacial defects. The interfacial defect criticality unveiled from this study can provide guidelines for maintenance when defect is detected during inspection and it can be beneficial to a more precise performance evaluation and service life prediction of FRP-bonded concrete structures.

1. Introduction

Fiber reinforced polymer (FRP) has been proven to be an efficient material to strengthen and/or retrofit deficient concrete components and structures through an external bonding technique. A lot of buildings, bridges and other concrete structures have been rehabilitated to date, providing an effective service life extension to deficient systems and a huge saving to the economy [1–6].

In spite of the wide application of the external bonding FRP technique, one major challenge still needs to be solved: the identification of potential defects that may arise during the designed service life. Defects from the construction process and/or environmental deterioration may easily occur during the service life of FRP-bonded concrete structures. It is important to clearly determine the defect effect to provide guidance for engineers to decide whether a defect found during inspection can be merely neglected as non-critical, or should be monitored for some time before repair is necessary, or has to be treated immediately. However, most existing experimental and numerical studies have focused on the strengthening of new structures, but limited research has been conducted on structures with defects [7–10]. The effect of different defects, such as concrete cavities, inadequate primer and excessive primer, on FRP-bonded concrete systems has been studied through a fracture mechanics approach [11]. The energy release rates of specimens with different defects were measured and compared to that of a control specimen. The experimental results have revealed that minor concrete cavities do not have an adverse effect on fracture toughness and the critical circular disbond size is the half

* Corresponding author. Department of Architecture and Civil Engineering, City University of Hong Kong, Hong Kong, China.
E-mail address: denvid@mit.edu (D. Lau).

The final version ofthis manuscript is available in COMPOSITES. PART B, ENGINEERING. DOI: 10.1016/j.compositesb.2016.12.055

of the FRP width. When slabs with different FRP bonding lengths were investigated, it was shown that the FRP bonding length can affect the load carrying capacity and ductility of the slab. The load capacity of a slab that was FRP-bonded at the ends was 21% lower than that of a slab fully bonded with FRP [12].

Among the different defect types that may occur in FRP-bonded concrete beams, interfacial defect at the bond region between FRP and concrete substrate is one of the most important type [13–17]. It has been demonstrated that the overall behavior of FRP-bonded concrete beams largely depends on the interface integrity and the bond performance between FRP and concrete [18–22]. The interfacial defect at the bond line may induce stress concentration, which may initiate local bond failure, and have a further adverse effect on the global strengthening performance.

There is one document providing guidance to designers and engineers on the criticality of interfacial defect, *i.e.* the Guide for the Design and Construction of Externally Bonded FRP Systems for Strengthening Concrete Structures from the American Concrete Institute (ACI) [23]. According to the ACI guidance, delamination is classified as small, medium or large depending on the delamination area. Small delamination whose area is less than two square inches is permissible provided that the delamination area is less than 5% of the entire laminate area. Medium delamination is in the range of 2–25 square inches. When the delamination area is greater than 25 square inches, it is classified as large and can influence the performance of FRP significantly. A repair should be performed through cutting away the affected part and applying overlapping FRP. Although there is an empirical agreement, the thresholds for critical defects and the influence of such defects on long term performance of FRP-bonded concrete systems are not sufficiently investigated. Thus, for the service of better durability, a comprehensive understanding and quantification of the interfacial defect effect are of great significance in the design and maintenance of FRP strengthened/rehabilitated concrete structures.

The objective of this study is to investigate interfacial defect criticality in FRP-bonded concrete beams in terms of location and size aspects. The properties of the constituent materials (*i.e.*, FRP, concrete and epoxy adhesive) are characterized experimentally. Then, the mechanical response and failure modes of FRP-bonded concrete beams with different defect sizes and locations are obtained by performing four-point bending tests. In order to study the size effect of FRP-bonded concrete beam, finite element models representing different sizes of FRP-bonded concrete beams are built and simulated. Finally, interfacial defect criticality in FRP-bonded concrete beams is summarized and recommended. It is envisioned that the interfacial defect criticality found in this study can enrich design guideline with a consideration of the interfacial defect effect and a more precise performance evaluation and service life prediction of FRP strengthened or retrofitted structures.

2. Materials and methods

2.1. FRP-bonded concrete samples and defect design

The concrete with Grade 40 was used in this work. Details of the concrete mix are shown in Table 1. Two kinds of concrete samples were cast, *i.e.* concrete cubes and concrete beams. The side length of concrete cubes is 150 mm. The dimensions of concrete beams are 100 × 100 × 500 mm corresponding to width × depth × length. All concrete samples were cured in 23 °C water tank for 28 days. After curing, the samples were taken out in lab condition for drying.

The unidirectional carbon FRP was used as external reinforcement. The coupon test of FRP was conducted to attain the tensile properties in longitudinal direction. The test was conducted in accordance with the Standard ASTM D3039.

Before bonding FRP to concrete, the surface preparation of concrete is very important to guarantee the quality and reliability of the bonding. The surface of the concrete should be sanded by the sandpaper and the extra dust should be blown away. Then the surface should be cleaned by industry alcohol to remove grease. After cleaning the surfaces of concrete, the Teflon tape was bonded to the designed location of concrete serving as the defect region. The Teflon tape can prevent the concrete surface from the epoxy adhesive so that the interfacial defect was fabricated. The interfacial defect was designed to be located at the mid-span or shear-span of the beam, which is shown in Fig. 1(a). The defect size was designed as 2000 mm^2, 4000 mm^2 and 6000 mm^2. The width of defect was 100 mm, which was same as the width of concrete beam. The beams were designed in the format of 'a-X-b' where 'a' stands for the beam length, 'X' represents the location of the interfacial defect (that is 'M' for mid-span and 'S' for shear-span), and 'b' denotes the size of interfacial defect. For example, 0.5-M-4000 means that the length of FRP strengthened concrete beam is 0.5 m, the interfacial defect is located at the mid-span of the beam and the defect size is 4000 mm^2. The FRP was bonded to the bottom surface of the concrete beams through epoxy, which suffers tension stress under four-point bending test. FRP was infiltrated by the epoxy and put on the concrete beams where the fiber direction was in align to the length of the beam. The epoxy applied here has been demonstrated high strength and it can provide good stress transfer from concrete to FRP. A uniform pressure was applied on the FRP to ensure that

FIG. 1

Table 1
Concrete mix design.

Concrete grade	Water/cement ratio	Sand/aggregate	Density (kg/m^3)	Specific weight (kg/m^3)		
				Cement	Sand	Aggregate
C 40	0.6	0.45	2374	383	792	968

The final version ofthis manuscript is available in COMPOSITES. PART B, ENGINEERING. DOI: 10.1016/j.compositesb.2016.12.055

the FRP and concrete were well bonded excluding the Teflon tape area. After 7 days curing, the FRP-bonded concrete beams were ready for test.

2.2. Test instrumentation

The concrete cubes were under compressive test to determine the properties of concrete. Before testing, the dimensions of concrete cube should be measured and the concrete cube should be placed at the center of sample stage. The loading speed was adopted as 13.5 kN/s according to the British Standard BS EN 12390. The load kept increasing until it reached the maximum value. The compressive strength of concrete can be calculated based on the dimensions and the load data acquired from the material test system.

The four-point bending test setup was used in this program. The support span length was 300 mm and the load span was 150 mm. The FRP-bonded concrete beams were loaded by a 100 kN actuator. The load was applied monotonically under displacement control at rate of 0.5 mm/min until failure. Two linear variable displacement transducers (LVDTs) were put in the middle of front and back side of beams to measure the mid-span displacement. Meanwhile, one strain gauge was bonded to the middle of the FRP and the other six strain gauges were evenly bonded to the left and right part of FRP surface to measure the FRP strain variations. The photo of four-point bending test setup is shown in Fig. 1(b). During the test, the load, mid-span displacement and FRP strain variations were measured and recorded simultaneously through TDS-303 Data Logger. All FRP-bonded concrete samples with different defect design were tested with the identical instrumentation.

3. Finite element modeling

The numerical analysis is carried out using the ABAQUS FE (finite element) software [24]. The boundary conditions, mechanical properties and load conditions of FE models are set based on the reported experiment in literature. The detailed information of the experimental specimen is given in Table 2, and the explicit setup of experimental test can be found in Ref. [25].

3.1. Modeling of concrete

The concrete is modeled using the plane stress element CPS4 (4-node bilinear). The concrete damaged plasticity model in ABAQUS is adopted to define the compressive and tensile behavior of concrete. The Poisson's ratio and the dilation angle for the concrete are set as 0.2 and 35°, respectively. For the concrete under uniaxial compression, the stress-strain relationship is defined based on Saenz's model [26], which can be described as follows:

$$\sigma = \frac{\alpha\varepsilon}{1 + \left[\left(\frac{\alpha\varepsilon_p}{\sigma_p}\right) - 2\right]\left(\frac{\varepsilon}{\varepsilon_p}\right) + \left(\frac{\varepsilon}{\varepsilon_p}\right)^2} \quad (1)$$

where σ is the compressive stress and ε is the corresponding compressive strain; σ_p is the maximum compressive stress of concrete which is set to compressive strength f_c' and the ε_p is the corresponding strain; α is the initial tangent modulus which is set as the elastic modulus of concrete E_c in absence of test data. The elastic modulus of concrete is estimated following the equation from ACI guideline, $E_c = 4730\sqrt{f_c'}$ [27].

The tensile behavior of concrete is defined as linear elastic up to the tensile strength (f_t), which can be estimated from the CEB-FIP equations [28]:

$$f_t = 1.4\left[\frac{(f_c' - 8)}{10}\right]^{\frac{2}{3}} \quad (2)$$

The post-failure tension stiffening model of concrete is then determined by the tension stiffening factor β and the tensile strength f_t [29–31]. The tension stiffening factor β can be determined by the following equation:

$$\beta = \exp\left[-1100(\varepsilon_{ct} - \varepsilon_{cr})\left(\frac{E_s}{200}\right)\right] \quad (3)$$

where E_s is the elastic modulus of reinforcement, ε_{cr} is the concrete strain at cracking and ε_{ct} is the corresponding tensile strain.

The post-failure tensile stress-strain behavior then can be determined as:

$$\sigma_{ct} = \beta f_t \quad (4)$$

where σ_{ct} is the tensile stress corresponding to the tensile strain ε_{ct}.

3.2. Modeling of steel and FRP reinforcements

The truss element T2D2 (2-node linear displacement) is used to model both the steel and FRP reinforcements. The nonlinear behavior of steel reinforcement is modeled as linear elastic up to yield stage, beyond which it is fully plastic. The FRP reinforcement is assumed to be linear elastic to failure, and the rupture point is set as the maximum tensile strength of the FRP.

3.3. Modeling of FRP-concrete interface

The bond-slip behavior of the FRP-concrete interface is simulated by the cohesive element COH2D2 (4-node, two-dimensional cohesive element). The interface damage initiation and propagation phase can be described by the traction-separation law defined to cohesive elements in ABAQUS. The bi-linear traction-separation law proposed by Lu is adopted in this study, which is one of the most accurate models to simulate the bond-slip behavior of the FRP-concrete interface [32,33]. The bilinear traction-separation law in the present FE study is shown in Fig. 2, and the parameters in this model are determined as follows:

Table 2
Geometry and material properties of beam models.

Beam details	Parameters	Value
Beam dimensions	Span l (mm)	3000
	Width b_c (mm)	203
	Depth d (mm)	406
Concrete	Cylinder compressive strength f_c' (MPa)	37.2
	Elastic modulus E_c (MPa)	28850
	Tensile Strength f_t (MPa)	2.86
Steel reinforcement	Tension bars/yield strength f_{yt} (Mpa)	2ϕ16/440
	Compression bars/yield strength f_{yc} (Mpa)	2ϕ9.5/440
	Stirrups/yield strength of stirrups f_{yv} (MPa)	7@102/596
	Elastic modulus of all steel bars E_s (GPa)	200
FRP reinforcement	Thickness t_f (mm)	1.19
	Width b_f (mm)	50
	Length L_f (mm)	2744
	Tensile strength f_{fu} (MPa)	2400
	Elastic modulus E_f (GPa)	155

Note: 1 In the symbol xϕy, x represents the number of the tension/compression bars and y represents the diameter of the tension/compression bars. 2 In symbol x@y, x stands for the diameter of the stirrups and y stands for the space between stirrups along the entire beam span.

The final version ofthis manuscript is available in COMPOSITES. PART B, ENGINEERING. DOI: 10.1016/j.compositesb.2016.12.055

FIG. 2

$$\tau = \frac{\tau_{max}\, s}{s_0} \quad \text{when } s \le s_0 \tag{5}$$

$$\tau = \frac{\tau_{max}\left(s_f - s\right)}{s_f - s_0} \quad \text{when } s_0 \le s \le s_f \tag{6}$$

$$\tau = 0 \quad \text{when } s \ge s_f \tag{7}$$

where

$$s_f = \frac{2G_f}{\tau_{max}} \tag{8}$$

$$\tau_{max} = 1.5\beta_w \times f_t \tag{9}$$

$$\beta_w = \sqrt{\frac{\left(2.25 - \frac{b_f}{b_c}\right)}{\left(1.25 + \frac{b_f}{b_c}\right)}} \tag{10}$$

$$s_0 = 0.0195\beta_w^2 \times \sqrt{f_t} \tag{11}$$

in which b_f and b_c are the width of FRP reinforcement and concrete beam, respectively; β_w is the width ratio between FRP and concrete and G_f is the interfacial fracture energy which can be written as:

$$G_f = 0.308\beta_w^2 \times \sqrt{f_t} \tag{12}$$

3.4. Specimen design

In total, fourteen beam models are built in ABAQUS, which can be divided into three groups for different purposes. One FRP-bonded reinforced concrete beam FE model, *i.e.* 3-M-0 (3-S-0), is designed exactly as the experimental setup to validate the FE simulation scheme against the experimental results. Six FRP-bonded reinforced concrete beam models in 3-m group are designed based on the reference case and they contain different defect arrangements at FRP-concrete interface. Beam models 3-M-6000, 3-M-12000 and 3-M-24000 refer to that the defect is located at mid-span with the size of 6000 mm^2, 12000 mm^2 and 24000 mm^2, respectively. Such defect size is designed based on the thresholds given by ACI 440.2R to evaluate the criticality of the delamination between external FRP reinforcement and concrete. In order to investigate the effect of defect criticality in terms of location, beam models 3-S-6000, 3-S-12000 and 3-S-24000 are built referring to the samples containing shear-span defect. To further study the effect of beam length on the interfacial defect criticality, seven 6-m beam models, 6-M-0 (6-S-0), 6-M-6000, 6-M-12000, 6-M-24000, 6-S-6000, 6-S-12000 and 6-S-24000 are built. The reinforcement setting and defect design are the same as those of 3-m group. Both the longitudinal reinforcement arrangement and cross-section design are the same as the experimental specimen so as to minimize the influence caused by other factors.

4. Results and discussions

4.1. Experimental results of FRP-bonded concrete beams

The compressive test is conducted with concrete cubes. The compressive strength and elastic modulus of concrete are 51.3 MPa and 29.7 GPa, respectively. The cracks in concrete under compression are in parallel to the applied load direction. The mechanical properties of FRP under tensile test are shown in Table 3. The tensile strength of FRP is 3.69 GPa (Standard deviation: 0.33 GPa). With such high tensile strength, FRP can provide efficient reinforcement for concrete beams. The epoxy is to integrate concrete and FRP along the interface. The epoxy used here is high strength and high modulus. The mechanical properties of epoxy are shown in Table 4.

The effect of interfacial defect is characterized by the mechanical properties of FRP-bonded concrete beams. The load-displacement behavior of FPR-bonded concrete beams containing interfacial defects at mid-span is shown in Fig. 3. The unstrengthened beam shows a linear response until peak beyond which a sudden load drop is reached, accompanied by the failure of the beam. The strengthened beams exhibit a similar response at the elastic stage. The load rises with the increase of mid-span displacement. Once the concrete reaches its stress limit, the load-displacement relation switches to cracking stage in which the stiffness is lower than that of elastic stage. Then, a linear ascent load-displacement behavior (which is defined to ultimate stage) is followed by a sudden load decline immediately after the peak load is reached, in which the failure happens. FRP-bonded concrete specimen in different stages is shown in Fig. 4. In the elastic stage, concrete is intact and the cracks occur in concrete once the concrete is beyond its stress limit. In cracking stage, the cracks propagate and FRP sheet withstands high tensile stress. Concrete at compression region has not reached the limit strain and cracks propagate to the top of the beam, which can be seen in Fig. 4 (b). Due to the presence of shear force, the concrete substrate slips slowly with the FRP. In ultimate stage, cracks continue to propagate and the ascending load-displacement behavior of specimen is attributed to the bond performance between concrete and FRP. With the increase of load, the slip between concrete and FRP reaches the limit and the specimen abruptly fails by the intermediate crack induced debonding.

The mechanical properties of FRP-bonded concrete beams with different arrangements of interfacial defect are shown in Table 5. The load capacity of FRP-bonded concrete beams is an important parameter indicating the mechanical property enhancement. The

Table 3
The mechanical properties of FRP.

Properties	Values	Notes
Tensile strength	3.69 GPa	The test followed the guideline of ASTM D3039
Ultimate strain	0.0158	
Elastic modulus	234 GPa	
Thickness	0.166 mm	

The final version ofthis manuscript is available in COMPOSITES. PART B, ENGINEERING. DOI: 10.1016/j.compositesb.2016.12.055

Table 4
Mechanical property of epoxy (from manufacturer).

Property	Result	Test method
Flexural strength (MPa)	79	ASTM D790
Flexural Modulus (GPa)	3.45	ASTM D790
Elongation	3%	ASTM D638
Service temperature (°C)	−40–60	–

FIG. 3

dissipated energy (U) of FRP-bonded concrete beams is composed of elastic energy stored in concrete and FRP, and inelastic energy for crack formation and propagation in concrete and interfacial bond between concrete and FRP. The dissipated energy can be quantified through integrating the area under load-displacement curve until peak load, which can be expressed as:

$$U = \int_0^{\Delta_u} P d\Delta \tag{13}$$

where Δ_u is the displacement at the peak load and P is the applied load. For the FRP-bonded concrete beams containing interfacial defects at mid-span, a slightly decreasing trend in load capacity (P_u) and ultimate displacement (Δ_u) is observed as the defect size increases from 2000 mm^2 to 6000 mm^2. When compared to reference beam (0.5-M-0), only 5% reduction in load capacity and 6% decrease in ultimate displacement is observed in 0.5-M-6000. A similar decrease in dissipated energy is observed with the increase of interfacial defect size. The average dissipated energy of beams with 6000 mm^2 defect is 12.4% lower than that of the reference beam (0.5-M-0).

Table 5
The mechanical properties of 0.5-m beams with different defect arrangements.

Beams designation	P_u(kN)	Δ_u(mm)	U (J)
0.5-M-0 (0.5-S-0)	75.4	1.95	89.6
0.5-M-2000	74.3	1.86	84.1
0.5-M-4000	71.9	1.88	81.0
0.5-M-6000	71.6	1.82	78.5
0.5-S-2000	67.2	1.61	63.0
0.5-S-4000	57.9	1.49	54.6
0.5-S-6000	40.0	1.15	30.9

When the interfacial defect is located at the shear-span of the FRP-bonded concrete beam, the load-displacement curves are shown in Fig. 5. The presence of an interfacial defect at the shear-span has a significant influence on the mechanical properties of FRP-bonded concrete beams. The interfacial defect of 2000 mm^2 size (0.5-S-2000) results in a reduction of 10.9% in capacity compared to that of sample 0.5-S-0. Such a reduction in load capacity increases to 46.9% and the dissipated energy decreases by 66.5% for beam 0.5-S-6000 compared to reference beam (0.5-S-0). As discussed in previous paragraph, the load capacity of FRP-bonded concrete beam in the ultimate stage is attributed to the bond strength between FRP and concrete. The observed reduction is due to the bond strength drop of FRP-concrete interface. The force for debonding FRP and concrete highly depends on the bond length. With the increase of bond length, the bond strength keeps increasing until reaching the effective bond length. The effective bond length is defined as the distance between the zero strain point at the far end of FRP sheet and maximum strain point. The effective bond length, L_e, can be determined through following equation:

$$L_e = 0.7\sqrt{\frac{E_f \cdot t_f}{c \cdot f_t}} \tag{14}$$

where E_f and t_f are the elastic modulus and thickness of FRP; f_t is the tensile strength of concrete and c is a constant which can be acquired through calibration with experimental results. For carbon FRP sheet, c is equal to 2. Once the bond length reaches the effective

FIG. 4

The final version ofthis manuscript is available in COMPOSITES. PART B, ENGINEERING. DOI: 10.1016/j.compositesb.2016.12.055

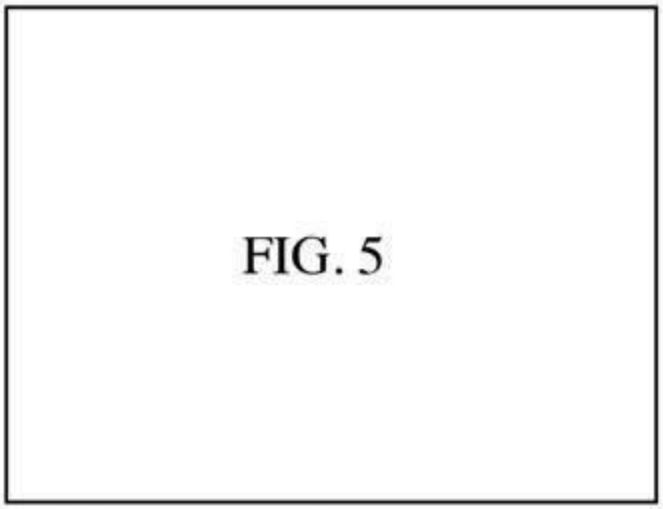

bond length, the load capacity does not tend to increase with the further extension of FRP. If the FRP bond length L_f is smaller than effective bond length, the corresponding ultimate debonding load, P_d, can be calculated based on:

$$P_d = P_{max} \cdot \frac{L_f}{L_e} \cdot \left(2 - \frac{L_f}{L_e}\right) \tag{15}$$

where P_{max} is the maximum debonding load in which the bond length is equal to effective bond length. Based on the materials properties, the effective bond length can be calculated. The bond length in FRP-bonded concrete beam is smaller than the effective bond length. Thus, the reduced bond length due to interfacial defect leads to a noticeable reduction in load capacity of FRP-bonded concrete beam. It should be noted that the variation of elastic stage and cracking stage in load-displacement curves of 0.5-S-2000, 0.5-S-4000 and 0.5-S-6000 is insignificant, proving that the bond performance of FRP-concrete interface is of crucial importance in providing stress transfer and overall behavior of FRP-bonded concrete beams. In the test, the support is in the direct contact with the FRP, increasing the end-anchorage capacity of FRP. In real strengthening application, enough FRP end anchorage should be ensured to avoid plate end debonding.

The failure mode of FRP-bonded concrete beams is composed of concrete fracture and intermediate FRP debonding. The FRP debonding initiates within the shear-span region due to the shear force and propagates along the FRP-concrete interface toward the direction of plate end. Strain development along the FRP sheet in different load levels, *i.e.* 25%P_u, 50%P_u, 75%P_u and 100%P_u, are shown in Fig. 6. Here, P_u is the maximum load for every FRP-bonded concrete beams that fail by debonding. The strain variations on FRP is important to evaluate the structural behavior of FRP-bonded concrete beams. A gradual increase of strain is observed with increasing load up to 75%P_u, while the increase rate of different beams is affected by the defect size. For instance, the strains of beam 0.5-S-2000 are always larger than those of 0.5-S-4000 and 0.5-S-6000 in all load levels, implying the stress transfer efficiency in 0.5-S-2000 is higher and the interface response controls the overall mechanical properties of FRP-bonded concrete beams. Besides, the strain can be used to analyze the interfacial shear stress between FRP and concrete. As the strain is a function of location x, the interfacial shear stress (τ) can be obtained as follows:

$$\tau = t_f \cdot E_f \cdot \frac{d\varepsilon}{dx} \tag{16}$$

where ε is the strain along the FRP. Only a slight deterioration on strain variations of 0.5-M-2000, 0.5-M-4000 and 0.5-M-6000 can be observed compared to those of 0.5-M-0 at different load levels. However, a much severer deterioration on strain is observed in 0.5-S-2000, 0.5-S-4000 and 0.5-S-6000 compared to those of reference beam, implying that the interfacial shear stress suffers a big loss. Meanwhile, it can be seen that the interfacial shear stress decreases rapidly with the increase of defect size from 2000 mm^2 to 6000 mm^2 in S series. It should be noted that the maximum strain observed during test (0.98%) is much lower than nominal rupture strain of FRP (1.58%), implying that FRP remains intact throughout the four-point bending test regardless of defect arrangement. Based on above results and discussions, it can be found that the defect at shear-span can induce local stress concentration near the defect, and possess a significant negative effect on the overall mechanical properties of FRP-bonded concrete beams.

4.2. Load-displacement behavior from FE model

The experimental data from a previous research is used to validate present finite element modeling [34]. The FRP-bonded reinforced concrete beam model with dimensions of 203 × 406 × 3000 mm is built, which is identical to the beams in the experiment. Fig. 7 shows the results of comparison between finite element simulation and experiment in terms of load-displacement curve for beam 3-M-0. Based on the results, the difference between the predicted and experimental load capacity is small and a good agreement between finite element prediction and experimental results is found. Thus, present finite element modeling is able to simulate the behavior of FRP-bonded concrete beams accurately.

The simulated applied load versus mid-span displacement curves of 3-m FRP-bonded concrete beams containing different interfacial defects are shown in Fig. 7. It can be easily seen that with the increase of defect size from 6000 to 24000 mm^2 at mid-span, the load capacity variations of FRP-bonded concrete beam are insignificant compared to that of the reference beam (3-M-0). The increase of interfacial defect size at mid-span results in an obvious reduction of ultimate displacement (Δ_u), up to 9.8% when the defect size reaches 24000 mm^2. When the defect is located at the shear-span, a serious deterioration in terms of load capacity (11.8%) and ultimate displacement (13.1%) is observed in 3-S-6000, implying that the tolerance for defect at shear-span is much lower than that of mid-span defect. As the size of shear-span defect increases from 6000 to 24000 mm^2, further degradation of load capacity and ultimate displacement is shown in 3-S-12000 and 3-S-24000. Moreover, the stiffness of load-displacement curves in ultimate stage shows a significant reduction compared to that of control beam (3-S-0). In ultimate stage, the FRP takes up growing load with the increase of mid-span displacement. The shear-span defect may induce local stress concentration near defect and has a big influence on the interfacial bond performance, further leading to the decreased load capacity and more brittle behavior of FRP-bonded concrete beam. Fig. 8 illustrates the crack pattern of 3-m FRP-bonded concrete beams containing 24000 mm^2 defect at mid-span or shear-span. It can be seen that the flexural cracks initiate in the high moment region and diagonal cracks initiate in the shear-span region, then diagonal cracks develop into the critical cracks, leading to the ultimate debonding failure of FRP-bonded concrete beam (part of FRP is detached from beam soffit). A summary of key mechanical properties of 3-m beams with different

The final version ofthis manuscript is available in COMPOSITES. PART B, ENGINEERING. DOI: 10.1016/j.compositesb.2016.12.055

FIG. 6

defect arrangements is illustrated in Table 6.

The load-displacement curves of 6-m FRP-bonded concrete beams containing different interfacial defects are illustrated in Fig. 9. The load-displacement behavior of beams containing different sizes of mid-span defects is close to that of control specimen (6-M-0). The maximum deviations of only 0.85% and 2.16% are found for beams with 24000 mm^2 mid-span defect in terms of load capacity and ultimate displacement compared to those of 6-M-0,

The final version ofthis manuscript is available in COMPOSITES. PART B, ENGINEERING. DOI: 10.1016/j.compositesb.2016.12.055

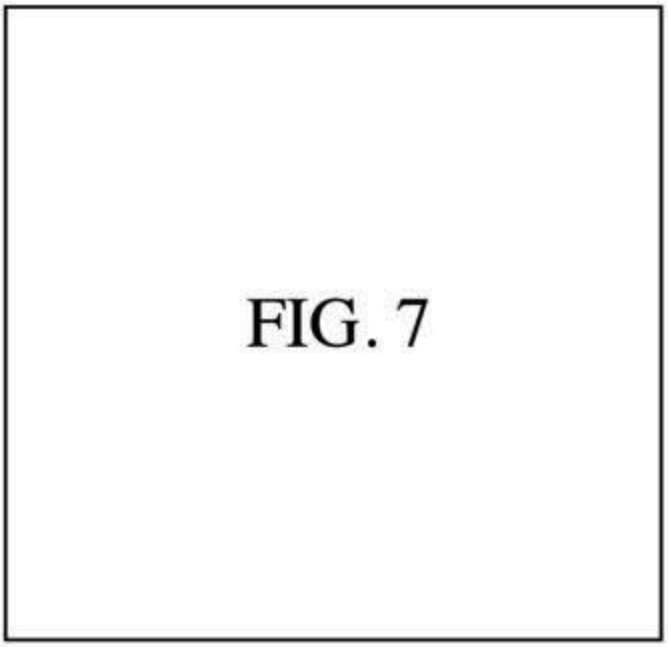

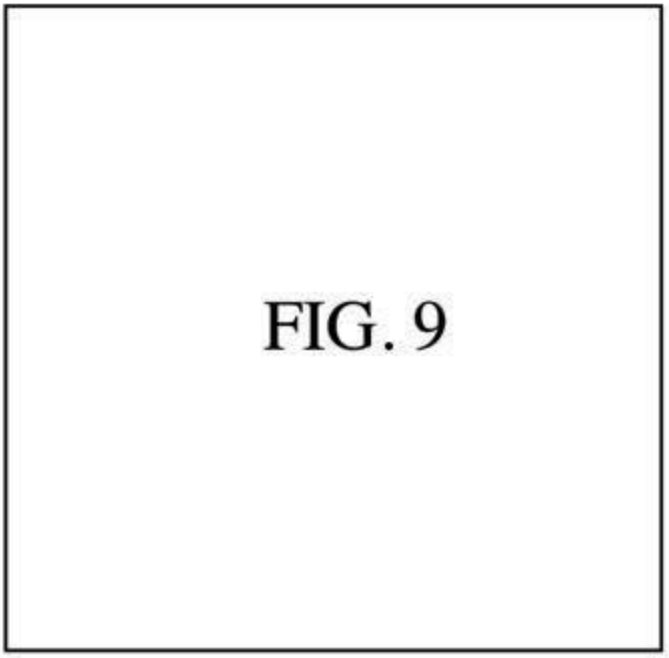

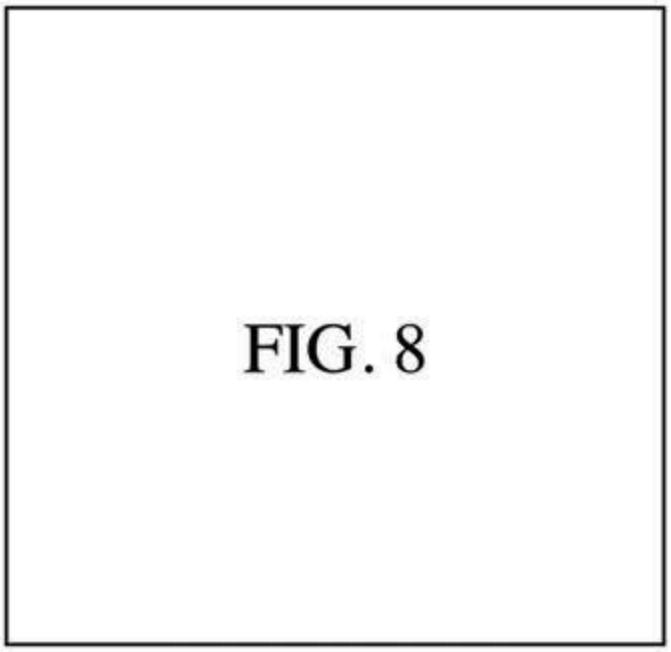

Table 6
The key mechanical properties of 3-m beam model with different defect arrangements.

Beams designation	P_u(kN)	$(P_{cu} - P_{du})/P_{cu}$	Δ_u(mm)	$(\Delta_{cu} - \Delta_{du})/\Delta_{cu}$
3-M-0 (3-S-0)	70.3	–	15.3	–
3 - M - 6000	69.7	0.85%	14.8	3.27%
3 - M - 12000	68.2	2.99%	14.4	5.88%
3 - M - 24000	67.6	3.84%	13.8	9.80%
3 - S - 6000	62.0	11.81%	13.3	13.07%
3 - S - 12000	60.2	14.37%	12.6	17.65%
3 - S - 24000	59.2	15.79%	12.5	18.30%

Note: P_{cu} and P_{du} are the load capacity of control beam and beams with interfacial defect, Δ_{cu} and Δ_{du} are the ultimate displacement of control beam and beams with interfacial defect.

respectively. For the beams containing defects at shear-span, the load-displacement behavior in elastic stage and cracking stage is quite similar to that of 6-S-0. However, a horizontal plateau is followed in the ultimate stage for beams with shear-span defect with the increase of displacement. This can be explained by the traction-separation law defined to the interfacial elements. The traction-separation law assumes that the interface does not resist any stress once the separation exceeds the critical value, resulting in a plateau provided that the bond length is sufficiently long. The effective bond length for this beam configuration is calculated as 115 mm according to Equation (14), implying that the load capacity variation of this group should be less noticeable as the FRP bond length in all beams is much larger than the effective bond length. The results show a trend that the loading capacity decreases slowly with the increase of interfacial defect size. The load capacity deterioration of 5.68%, 6.82% and 8.81% is observed corresponding to beams with 6000, 12000, 24000 mm^2 shear-span defect compared to that of 6-S-0. This phenomenon is evident in the results of 6-m FRP-bonded concrete beams, which is shown in Table 7. The crack patterns of 6-m FRP-bonded concrete beams with 24000 mm^2 interfacial defect at mid-span or shear-span are shown in Fig. 10. It can be seen that the flexural cracks initiate in the high moment region become more important for the 6-m beam scenario. The tolerance for interfacial defect at shear-span in 6-m beam scenario is larger than that of 0.5-m scenario.

4.3. Size effect of FRP-bonded concrete beam

When the size of FRP-bonded concrete beam increases from 0.5 m to 6 m, the load capacity ratio of beams containing 6000 mm^2 to corresponding control beam is shown in Fig. 11. From the figure, it can be seen that the effect of mid-span interfacial defect on overall load capacity is limited, and the interfacial defect at shear-span has a greater influence on the overall load capacity, especially for the 0.5-m beam scenario. The 6000 mm^2 interfacial defect at shear-span results in the load capacity deterioration, up to 46.9% for 0.5-m beam scenario. This drastic deterioration may attribute to the following two reasons. First, the 0.5-m FRP-bonded concrete specimen belongs to the deep beam in which the span-to-depth ratio (l/d) is equal to or less than four according to Standard ACI 318. The governing factor for the deep beam is its shear performance and shear strength of FRP-bonded concrete sample largely

The final version ofthis manuscript is available in COMPOSITES. PART B, ENGINEERING. DOI: 10.1016/j.compositesb.2016.12.055

Table 7
The key mechanical properties of 6-m beam model with different defect arrangements.

Beams designation	P_u(kN)	$(P_{cu} - P_{du})/P_{cu}$	Δ_u(mm)	$(\Delta_{cu} - \Delta_{du})/\Delta_{cu}$
6-M-0 (6-S-0)	35.2	–	60.2	–
6 - M -6000	35.1	0.28%	59.7	0.83%
6 - M - 12000	35.0	0.57%	59.4	1.33%
6 - M - 24000	34.9	0.85%	58.9	2.16%
6 - S -6000	33.2	5.68%	55.7	7.48%
6 - S - 12000	32.8	6.82%	54.0	10.30%
6 - S - 24000	32.1	8.81%	52.8	12.29%

Note: $P_{cu}$and $P_{du}$are the load capacity of control beam and beams with interfacial defect; $\Delta_{cu}$and $\Delta_{du}$are the ultimate displacement of control beam and beams with interfacial defect.

fig. 10

fig. 11

depends on the interfacial bonding. Second, the presence of interfacial defect at shear-span decreases the bond length significantly, resulting in remarkable deterioration of interfacial bond performance especially when the bond length is smaller than effective bond length. When it comes to the 3-m (l/d=7) and 6-m (l/d=14) beams, the bond length is sufficiently large compared to effective bond length. The 6000 mm^2 interfacial defect has a limited effect, only 11.8% and 5.7% deterioration in terms of the load capacity.

5. Recommendations and future work

According to the ACI 440.2R, delamination in FRP-bonded concrete system is classified as small, medium or large only considering the size [23]. Small delamination represents the size that is less than two square inches, and medium delamination is in the range of 2–25 square inches. Delamination size that is larger than 25 square inches belongs to large category. However, it is not accurate to evaluate defect criticality solely from size aspect as the defect location also plays an important role in defect effect.

Based on the experimental and numerical results in this study, it is recommended that small, medium and large defect categories are classified according to the defect location, beam type and defect size sequentially after an interfacial defect is detected in FRP-bonded concrete beam during inspection. Corresponding maintenance strategies and treatment methods should be adopted based on the category of detected defect. The flowchart of defect classification is shown in Fig. 12. The initial step is to identify that the location of defect falls into mid-span or shear-span region. Then, the beam type, *i.e.* deep beam or normal beam, should be determined according to the span-to-depth ratio (l/d). The deep beam refers to the beam whose l/d is equal to or less than four. According to the Eurocode 2, the l/d should be equal to or less than 15 in the design of reinforced concrete beam [35]. Thus, normal beam represents the beam whose span-to-depth ratio (l/d) is in the range of 4–15. Finally, the classification of defect can be determined according to the defect size. The criterion for "small" defect is that both the deterioration of load capacity and ultimate displacement are smaller than 10% compared to those of control specimen. The small defect can be neglected as its effect is insignificant. Once the deterioration of load capacity or ultimate displacement is higher than 20%, the defect should be evaluated as "large". The large defect affects the overall performance of entire system significantly and it should be repaired immediately through cutting away the affected region and applying an overlapping FRP sheet. The other defect is evaluated as "medium" and it may be repaired by resin injection or ply replacement in order to prevent the further expansion or enlargement of defect area.

In real FRP strengthening applications, the FRP anchorage also plays an important role as plate end debonding may arise due to the insufficient FRP anchorage. The anchorage type of FRP laminate and

The final version ofthis manuscript is available in COMPOSITES. PART B, ENGINEERING. DOI: 10.1016/j.compositesb.2016.12.055

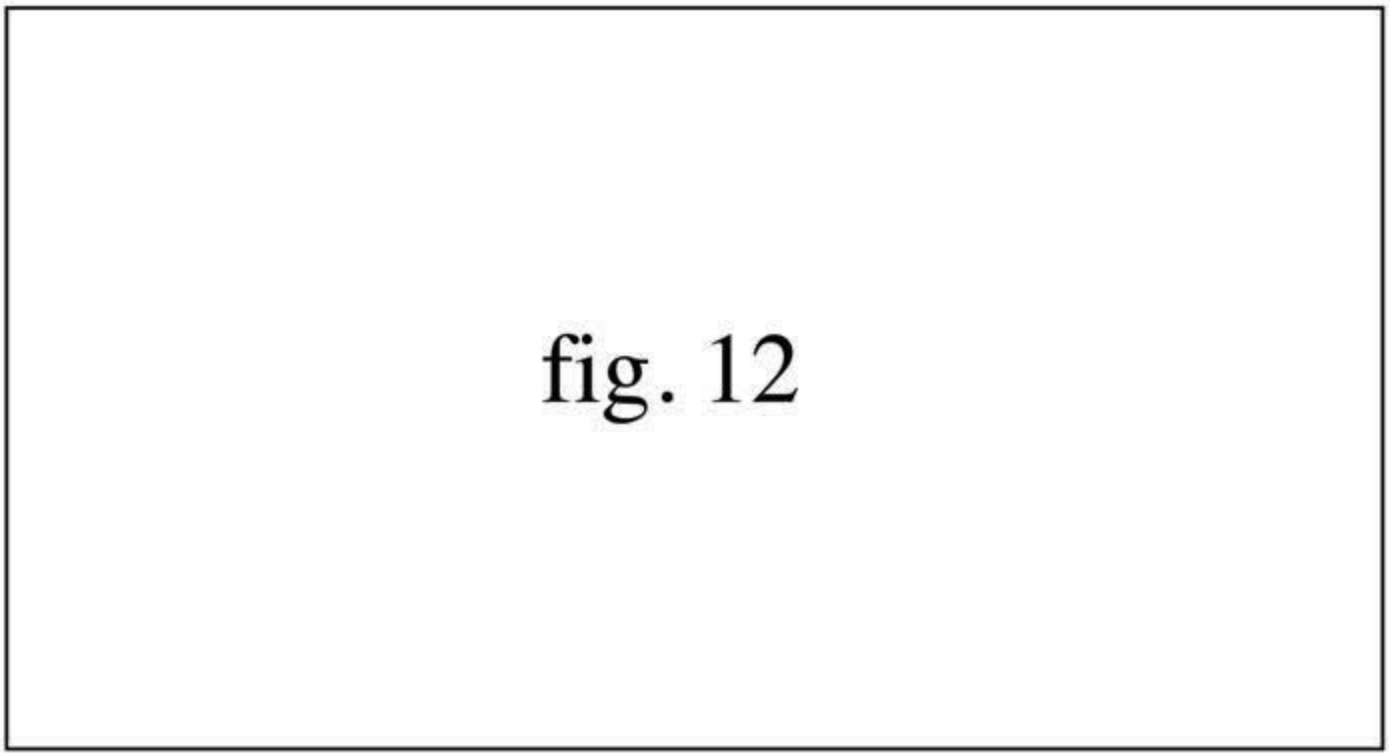

end-anchorage bond length are vital factors for the end-anchorage capacity and they may affect the mechanical properties of FRP-bonded concrete beams. The effect of FRP anchorage is recommended to be studied in the further work. During the service life, structures may experience a number of loading cycles and the behavior of FRP-bonded concrete structures under fatigue loading should be well considered. The application of cyclic loading may result in the loss of stiffness and accumulation of deflection. During the cyclic loading, flexural cracks initiate, the reinforcing bars slip at the crack position and the debonding of FRP laminates develops progressively. Moreover, when subjected to fatigue loading, a decrease of shear stress at the concrete-FRP interface is observed due to the slippage over time [36–40]. Based on these findings, further investigation on the fatigue loading effect should be conducted and more conservative upper size limits on the detected interfacial defect can be determined.

6. Conclusion

The criticality of interfacial defect between concrete and FRP was studied experimentally and numerically from the perspective of defect location and defect size. It is found that 6000 mm^2 interfacial defect at mid-span results in 5%, 0.85% and 0.28% deterioration in terms of load capacity corresponding to 0.5-m, 3-m and 6-m beams. When the defect is located at shear-span, the load capacity deterioration expands to 46.9%, 11.8% and 5.68% in 0.5-m, 3-m and 6-m beams respectively. The results reveal that the interfacial defect at shear-span is more critical than the defect at mid-span in FRP-bonded concrete beam in general. Moreover, the deep beam is more sensitive to interfacial defect than normal beam. The thresholds given by ACI 440.2R for small and large delamination are 2 in^2 and 25 in^2 respectively, which are too conservative according to the experimental observation and simulation results. The thresholds of small delamination for mid-span location can be enlarged to 6000 mm^2 and 24000 mm^2 for deep beam and normal beam, respectively. The thresholds of small and large delamination for shear-span location can be revised to 2000 mm^2 and 6000 mm^2 for the deep beam, and to 6000 mm^2 and 24000 mm^2 for the normal beam. After distinguishing the delamination as small, medium or large category, the corresponding maintenance strategies and treatment methods can be applied for the safety and durability of FRP-bonded concrete systems. The size and location aspects of interfacial defect criticality found from this study can act as a foundation for a more precise performance evaluation and a more reliable structural maintenance strategy.

Acknowledgements

The authors are grateful to the support from Croucher Foundation through the Start-up Allowance for Croucher Scholars with the Grant No. 9500012, and the support from the Research Grants Council (RGC) in Hong Kong through the General Research Fund (GRF) with the Grant No. 11255616.

References

[1] Seo S-Y, Lee MS, Feo L. Flexural analysis of RC beam strengthened by partially de-bonded NSM FRP strip. Compos Part B Eng 2016;101:21–30.
[2] Kim S-W, Park W-S, Jang Y-I, Feo L, Yun H-D. Crack damage mitigation and shear behavior of shear-dominant reinforced concrete beams repaired with strain-hardening cement-based composite. Compos Part B Eng 2015;79:6–19.
[3] Buyukozturk O, Gunes O, Karaca E. Progress on understanding debonding problems in reinforced concrete and steel members strengthened using FRP composites. Constr Build Mater 2004;18(1):9–19.
[4] Lau D, Qiu Q, Zhou A, Chow CL. Long term performance and fire safety aspect of FRP composites used in building structures. Constr Build Mater 2016;126:573–85.
[5] Aprile A, Feo L. Concrete cover rip-off of R/C beams strengthened with FRP composites. Compos Part B Eng 2007;38(5):759–71.
[6] Seo S-Y, Feo L, Hui D. Bond strength of near surface-mounted FRP plate for retrofit of concrete structures. Compos Struct 2013;95:719–27.
[7] Ueda T, Dai J. Interface bond between FRP sheets and concrete substrates: properties, numerical modeling and roles in member behaviour. Prog Struct Eng Mater 2005;7(1):27–43.
[8] Zhou A, Tam L-h, Yu Z, Lau D. Effect of moisture on the mechanical properties of CFRP–wood composite: an experimental and atomistic investigation. Compos Part B Eng 2015;71:63–73.
[9] Chen G, Teng J, Chen J. Finite-element modeling of intermediate crack debonding in FRP-plated RC beams. J Compos Constr 2010;15(3):339–53.
[10] Wu YF, Jiang C. Quantification of bond-slip relationship for externally bonded

The final version ofthis manuscript is available in COMPOSITES. PART B, ENGINEERING. DOI: 10.1016/j.compositesb.2016.12.055

FRP-to-concrete joints. J Compos Constr 2013;17(5):673–86.
[11] Karbhari VM, Navada R. Investigation of durability and surface preparation associated defect criticality of composites bonded to concrete. Compos Part A Appl Sci Manuf 2008;39(6):997–1006.
[12] Seim W, Hörman M, Karbhari V, Seible F. External FRP poststrengthening of scaled concrete slabs. J Compos Constr 2001;5(2):67–75.
[13] Lau D, Büyüköztürk O. Fracture characterization of concrete/epoxy interface affected by moisture. Mech Mater 2010;42(12):1031–42.
[14] Gunes O, Lau D, Tuakta C, Büyüköztürk O. Ductility of FRP–concrete systems: investigations at different length scales. Constr Build Mater 2013;49:915–25.
[15] Yu T, Cheng TK, Zhou A, Lau D. Remote defect detection of FRP-bonded concrete system using acoustic-laser and imaging radar techniques. Constr Build Mater 2016;109:146–55.
[16] Yuan H, Lu X, Hui D, Feo L. Studies on FRP-concrete interface with hardening and softening bond-slip law. Compos Struct 2012;94(12):3781–92.
[17] Ascione L, Berardi V, Feo L, Mancusi G. A numerical evaluation of the interlaminar stress state in externally FRP plated RC beams. Compos Part B Eng 2005;36(1):83–90.
[18] **Zhou A, Lau D. The Interfacial defect criticality of FRP strengthened concrete beams. In: Proceedings of the 24th International Conference on Composites/ Nano-Engineering. Hainan Island, China, Conference 17–23 July, Conference 2016.**
[19] **Zhou A, Lau D. Defect criticality of FRP-bonded concrete systems. In: Proceedings of the 2nd International Conference on Sustainable Urbanization. Hong Kong, Conference 7–9 January, Conference 2015.**
[20] Karbhari VM. Materials considerations in FRP rehabilitation of concrete structures. J Mater Civ Eng 2001;13(2):90–7.
[21] Tam L-h, Zhou A, Yu Z, Qiu Q, Lau D. Understanding the effect of temperature on the interfacial behavior of CFRP-wood composite via molecular dynamics simulations. Compos Part B Eng 2017;109:227–37.
[22] Ascione L, Feo L. Modeling of composite/concrete interface of RC beams strengthened with composite laminates. Compos Part B Eng 2000;31(6): 535–40.
[23] ACI 440.2R-02. Guide for the design and construction of externally bonded FRP systems for strengthening concrete structures, vol. 440. American Concrete Institute(ACI) Committee; 2002.
[24] Hibbett, Karlsson, Sorensen. ABAQUS/standard: User's Manual: Hibbitt, Karlsson & Sorensen. 1998.
[25] Brena SF, Bramblett RM, Wood SL, Kreger ME. Increasing flexural capacity of reinforced concrete beams using carbon fiber-reinforced polymer composites. ACI Struct J 2003;100(1):36–46.
[26] Saenz L. Discussion of "Equation for the stress-strain curve of concrete". J Am Concr Inst 1964;61(9):1229–35.
[27] ACI 318-08. Building code requirements for structural concrete and commentary, vol. 318. American Concrete Institute(ACI) Committee; 2008.
[28] CEB-FIP. CEB-FIP Model Code 90. London: Thomas Telford; 1993.
[29] Bischoff PH, Paixao R. Tension stiffening and cracking of concrete reinforced with glass fiber reinforced polymer (GFRP) bars. Can J Civ Eng 2004;31(4): 579–88.
[30] Qin R, Zhou A, Lau D. Effect of reinforcement ratio on the flexural performance of hybrid FRP reinforced concrete beams. Compos Part B Eng 2017;108: 200–9.
[31] Caporale A, Feo L, Luciano R. Damage mechanics of cement concrete modeled as a four-phase composite. Compos Part B Eng 2014;65:124–30.
[32] Lu X, Teng J, Ye L, Jiang J. Bond–slip models for FRP sheets/plates bonded to concrete. Eng Struct 2005;27(6):920–37.
[33] Lu X, Teng J, Ye L, Jiang J. Intermediate crack debonding in FRP-strengthened RC beams: FE analysis and strength model. J Compos Constr 2007;11(2): 161–74.
[34] Chen G, Teng J, Chen J, Xiao Q. Finite element modeling of debonding failures in FRP-strengthened RC beams: a dynamic approach. Comput Struct 2015;158:167–83.
[35] Institution BS. Eurocode 2: Design of Concrete Structures: Part 1–1: General Rules and Rules for Buildings. British Standards Institution; 2004.
[36] Yun Y, Wu YF, Tang WC. Performance of FRP bonding systems under fatigue loading. Eng Struct 2008;30(11):3129–40.
[37] Charalambidi BG, Rousakis TC, Karabinis AI. Fatigue behavior of large-scale reinforced concrete beams strengthened in flexure with fiber-reinforced polymer laminates. J Compos Constr 2016;20(5). 04016035.
[38] Oudah F, El-Hacha R. Research progress on the fatigue performance of RC beams strengthened in flexure using Fiber Reinforced Polymers. Compos Part B Eng 2013;47:82–95.
[39] Charalambidi BG, Rousakis TC, Karabinis AI. Analysis of the fatigue behavior of reinforced concrete beams strengthened in flexure with fiber reinforced polymer laminates. Compos Part B Eng 2016;96:69–78.
[40] Lau K, Dutta P, Zhou L, Hui D. Mechanics of bonds in an FRP bonded concrete beam. Compos Part B Eng 2001;32(6):491–502.

The final version ofthis manuscript is available in COMPOSITES. PART B, ENGINEERING. DOI: 10.1016/j.compositesb.2016.12.055

FIGURES

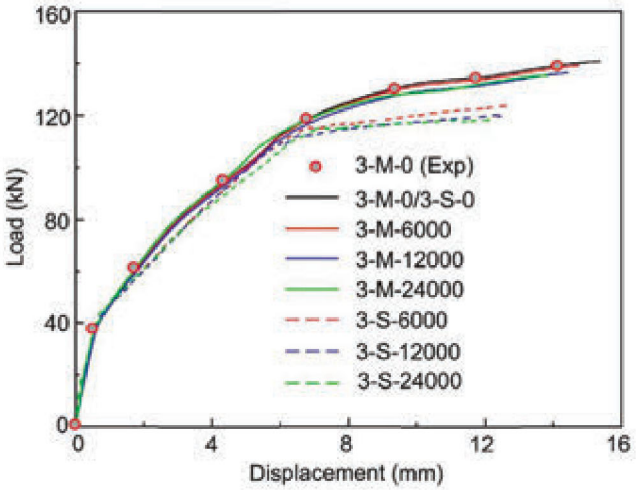

Fig. 7. The load-displacement behavior of 3-m length FRP-bonded concrete beams containing interfacial defect at mid-span and shear-span. The increase of interfacial defect size at mid-span results in an obvious reduction of ultimate displacement (Δ_u), up to 9.8% when the defect size reaches 24000 mm^2. When the defect is located at the shear-span, a serious deterioration in terms of load capacity (11.8%, 14.4% and 15.8%) and ultimate displacement (13.1%, 17.7% and 18.3%) is observed in 3-S-6000, 3-S-12000 and 3-S-24000, respectively. This implies that the tolerance for defect at shear-span is much lower than that of mid-span defect.

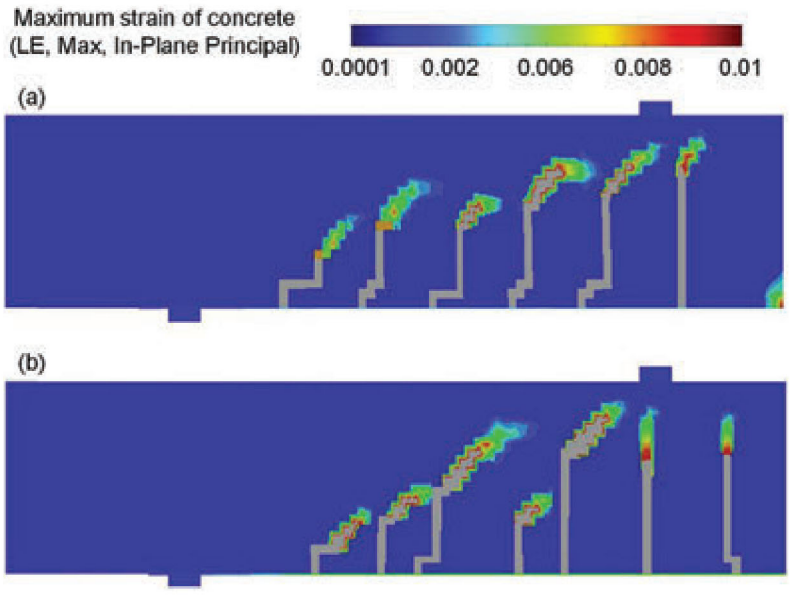

Fig. 8. FE crack patterns at ultimate load for 3-m length specimens: (a) interfacial defect at mid-span and (b) interfacial defect at shear-span. The flexural cracks initiate in the high moment region and diagonal cracks initiate in the shear-span region, then diagonal cracks develop into the critical cracks, leading to the ultimate debonding failure of FRP-bonded concrete beam (part of FRP is detached from beam soffit).

FIGURES

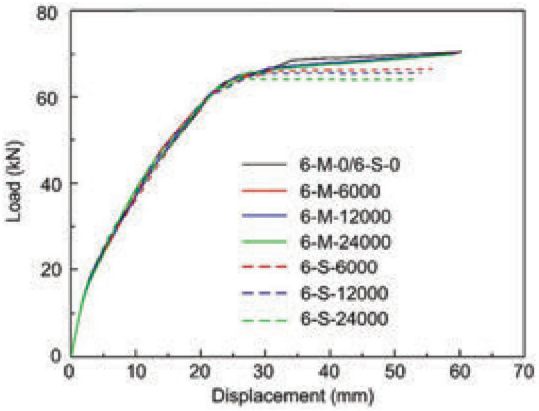

Fig. 9. The load-displacement behavior of 6-m FRP-bonded concrete beams containing interfacial defect at mid-span and shear-span. The maximum deterioration of 0.85% in load capacity and 2.16% in ultimate displacement are found for beams with 24000 mm^2 mid-span defect. The 5.68%, 6.82% and 8.81% load capacity deterioration are observed corresponding to beams with 6000, 12000, 24000 mm^2 shear-span defect. The tolerance for defect at longer beam is higher when the FRP bond length is larger than the effective bond length.

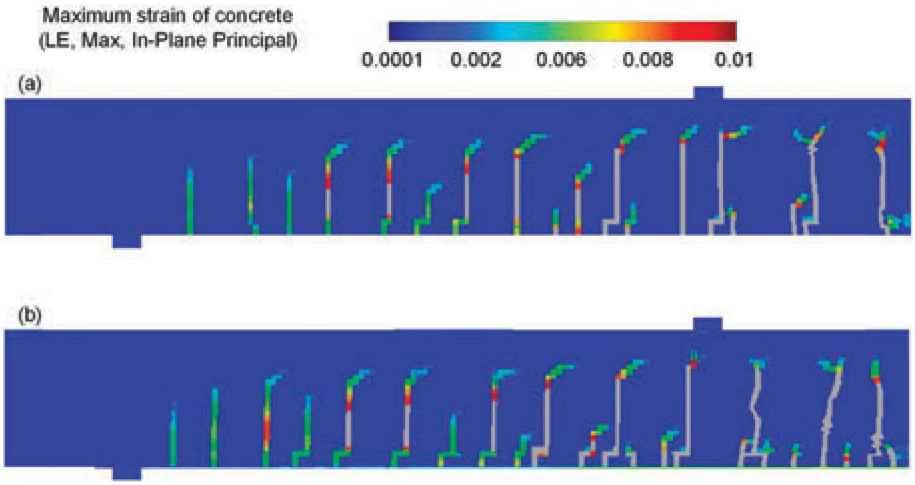

Fig. 10. FE crack patterns at ultimate load for 6-m specimens: (a) interfacial defect at mid-span and (b) interfacial defect at shear-span. The flexural cracks initiate in the high moment region become more critical for the 6-m beam scenario, implying that the tolerance for interfacial defect at shear-span is much larger than that of 0.5-m scenario.

FIGURES

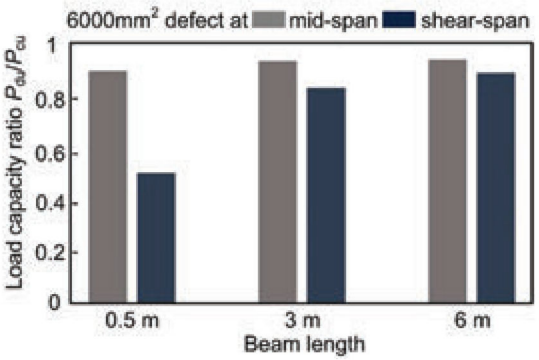

Fig. 11. The load capacity ratio of FRP-bonded concrete beams containing 6000 mm^2 interfacial defect (P_{du} and P_{cu} refer to the load capacity of the beam with interfacial defect and control beam). The effect of 6000 mm^2 interfacial defect at mid-span on the load capacity of beams is limited. The interfacial defect at shear-span has a more remarkable influence on the interfacial bond performance, causing the loss of global load capacity, especially for the deep beam scenario.

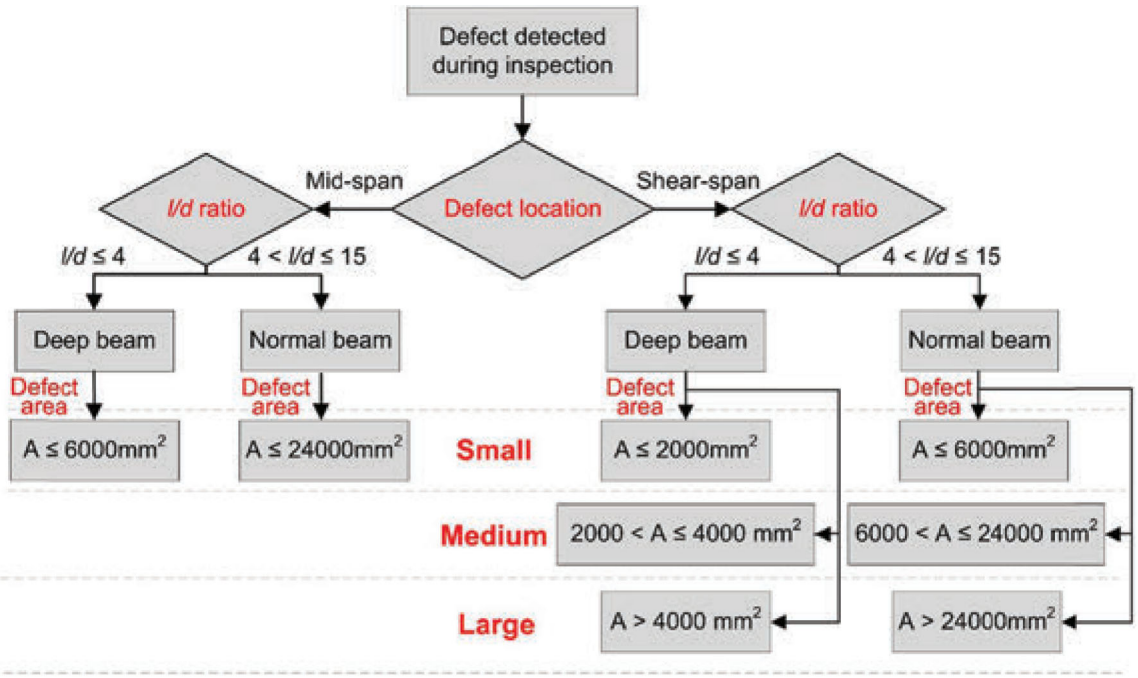

Fig. 12. The flowchart of defect classification. The defect location, beam type and defect size should be determined sequentially to evaluate the type of defect.

FIGURES

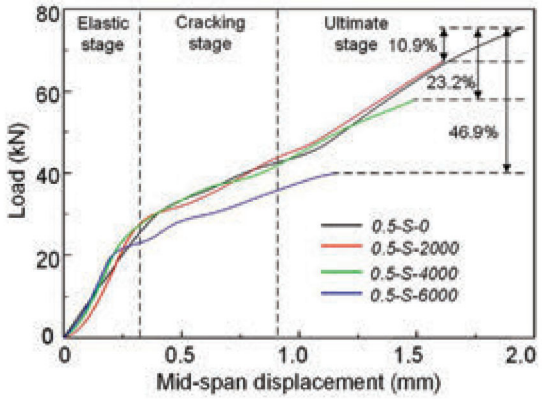

Fig. 5. The load-displacement behavior of FRP-bonded concrete beams containing interfacial defect at shear-span. The interfacial defect at shear-span results in 10.9%. 23.2% and 46.9% deterioration in load capacity corresponding to 2000, 4000 and 6000 mm^2 defect size, respectively.

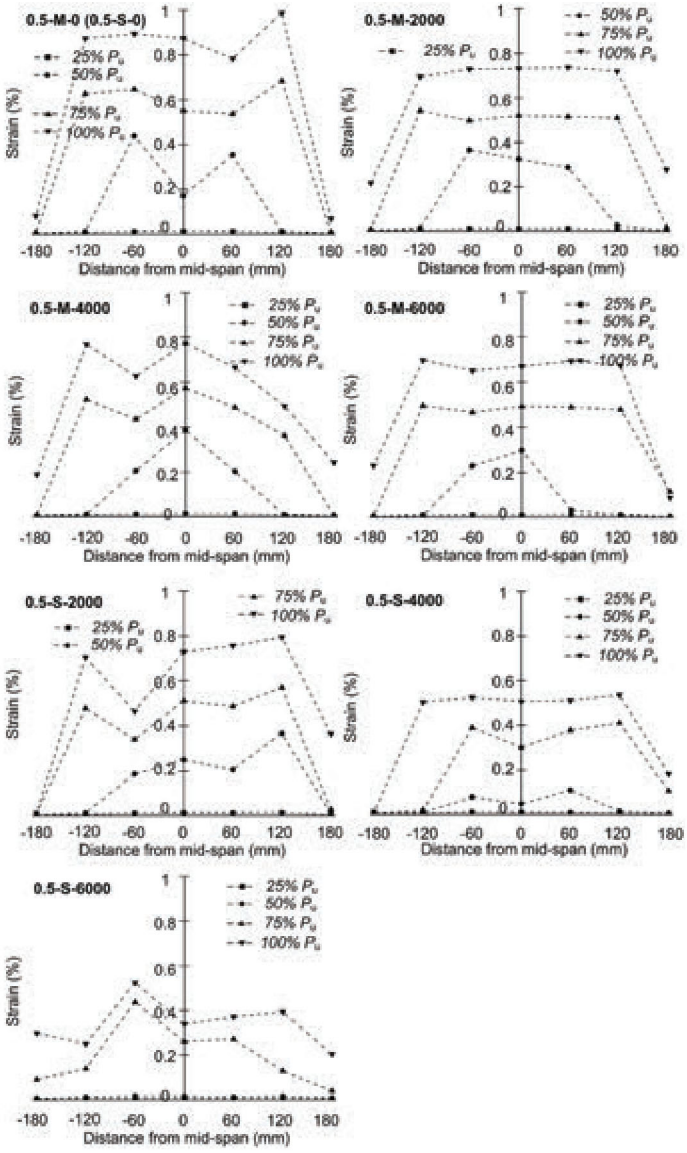

Fig. 6. The measured strain variations along FRP of samples: reference 0.5-M-0 (0.5-S-0); 0.5-M-2000; 0.5-M-4000; 0.5-M-6000; 0.5-S-2000; 0.5-S-4000 and 0.5-S-6000. The interfacial shear stress can be evaluated according to the strain variations on FRP. The interfacial defect at shear-span decreases stress transfer efficiency, induces the reduction of interfacial shear stress and further results in the deterioration of global performance of FRP-bonded concrete beams.

FIGURES

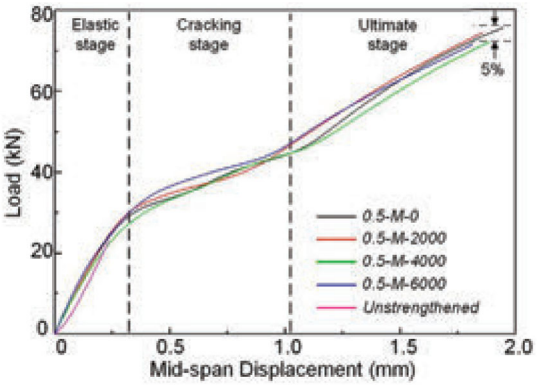

Fig. 3. The load-displacement behavior of FRP-bonded concrete beams containing interfacial defect at mid-span. With the increase of defect size from 2000 to 6000 mm^2 at mid-span, the maximum deterioration in terms of load capacity is only 5%, implying the effect of 6000 mm^2 interfacial defect at mid-span is not significant.

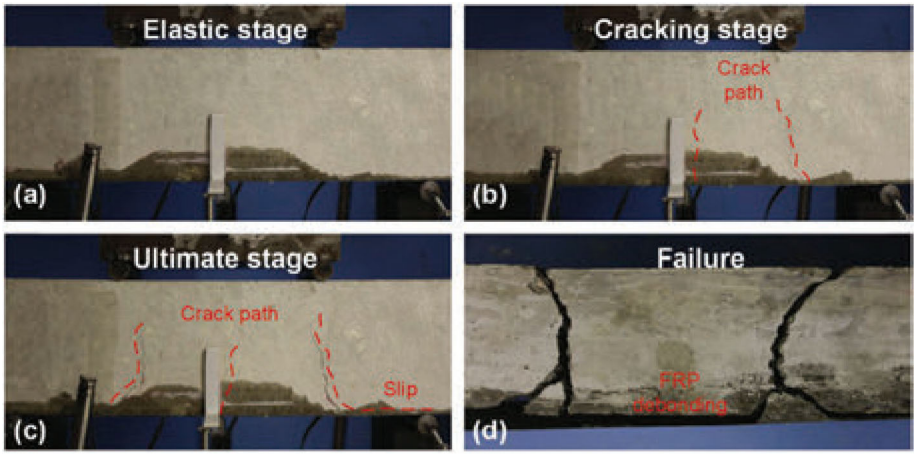

Fig. 4. FRP-bonded concrete specimen in different stages.

FIGURES

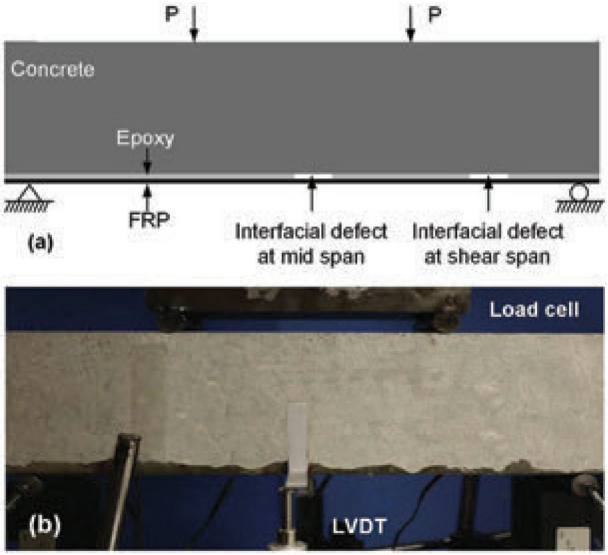

Fig. 1. (a) The arrangement of interfacial defect on FRP-bonded concrete specimen; (b) The photo of four-point bending test.

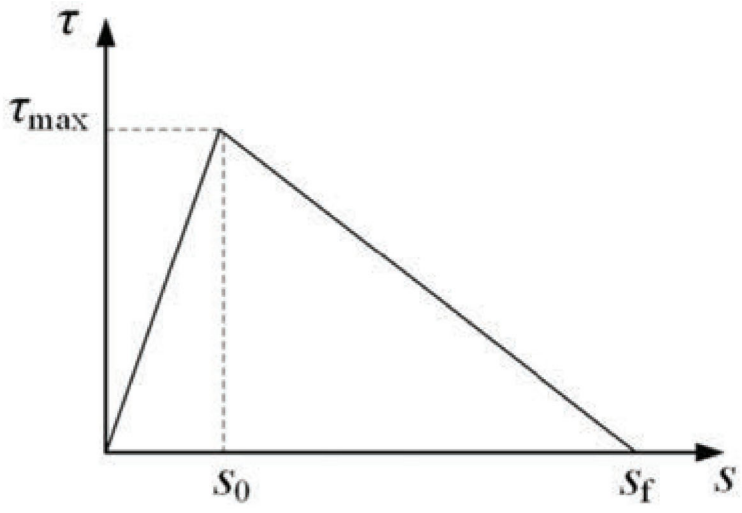

Fig. 2. The bilinear traction-separation law used to define the bond-slip behavior between FRP reinforcement and concrete.